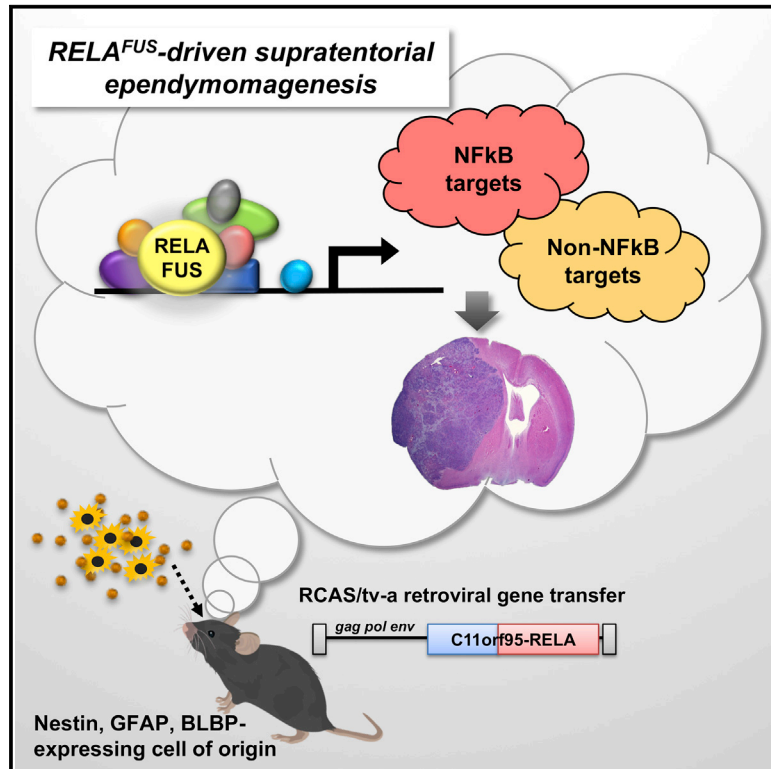# A *De Novo* Mouse Model of C11orf95-RELA Fusion-Driven Ependymoma Identifies Driver Functions in Addition to NF-κB

Graphical Abstract

Authors

Tatsuya Ozawa, Sonali Arora, Frank Szulzewsky, ..., David W. Ellison, Richard J. Gilbertson, Eric C. Holland

Correspondence

richard.gilbertson@cruk.cam.ac.uk (R.J.G.), eholland@fredhutch.org (E.C.H.)

In Brief

The C11orf95-RELA fusion (RELA^FUS) has been found in a distinct subset of supratentorial ependymomas. Ozawa et al. show that RELA^FUS is sufficient to drive ST-ependymoma formation from periventricular neural stem cells in mice. Furthermore, they show that RELA^FUS-induced tumorigenesis might depend on other cell signaling pathways in addition to NF-κB.

Highlights

- *RELA^FUS1* causes formation of mouse tumors that recapitulate ST-ependymoma histology

- The mouse tumors express a transcriptome similar to human ST-EPN-RELA tumors

- *RELA^FUS1* induces other signaling pathways in addition to canonical NF-κB signaling

- The ventricular wall is the putative location for ependymomagenesis of these tumors

Data and Software Availability

GSE93765

Article

A *De Novo* Mouse Model of C11orf95-RELA Fusion-Driven Ependymoma Identifies Driver Functions in Addition to NF-κB

Tatsuya Ozawa,[1,2,3,4] Sonali Arora,[1] Frank Szulzewsky,[1] Gordana Juric-Sekhar,[5] Yoshiteru Miyajima,[6] Hamid Bolouri,[1] Yoshie Yasui,[6] Jason Barber,[7] Robert Kupp,[8] James Dalton,[9] Terreia S. Jones,[10] Mitsutoshi Nakada,[11] Toshihiro Kumabe,[6] David W. Ellison,[9] Richard J. Gilbertson,[8,*] and Eric C. Holland[1,2,3,7,12,*]

[1]Division of Human Biology, Fred Hutchinson Cancer Research Center, University of Washington, Seattle, WA 98109, USA
[2]Seattle Tumor Translational Research (STTR), Fred Hutchinson Cancer Research Center, University of Washington, Seattle, WA 98109, USA
[3]Alvord Brain Tumor Center, University of Washington, Seattle, WA 98109, USA
[4]Division of Brain Tumor Translational Research, National Cancer Center Research Institute, Tokyo 104-0045, Japan
[5]Department of Pathology, University of Washington, Seattle, WA 98104, USA
[6]Department of Neurosurgery, Kitasato University School of Medicine, Sagamihara, Kanagawa 252-0374, Japan
[7]Department of Neurosurgery, University of Washington, Seattle, WA 98109, USA
[8]Cancer Research UK Cambridge Institute, University of Cambridge, Cambridge, UK
[9]Department of Pathology, St. Jude Children's Research Hospital, Memphis, TN 38105, USA
[10]University of Tennessee Health Science Center, Department of Clinical Pharmacy, Memphis, TN 39103, USA
[11]Department of Neurosurgery, Graduate School of Medical Science, Kanazawa University, Kanazawa, Ishikawa 920-8641, Japan
[12]Lead Contact
*Correspondence: richard.gilbertson@cruk.cam.ac.uk (R.J.G.), eholland@fredhutch.org (E.C.H.)
https://doi.org/10.1016/j.celrep.2018.04.099

SUMMARY

The majority of supratentorial ependymomas (ST-ependymomas) have few mutations but frequently display chromothripsis of chromosome 11q that generates a fusion between *C11orf95* and *RELA* (*RELA^FUS^*). Neural stem cells transduced with *RELA^FUS^* *ex vivo* form ependymomas when implanted in the brain. These tumors display enhanced NF-κB signaling, suggesting that this aberrant signal is the principal mechanism of oncogenesis. However, it is not known whether *RELA^FUS^* is sufficient to drive *de novo* ependymoma tumorigenesis in the brain and, if so, whether these tumors also arise from neural stem cells. We show that *RELA^FUS^* drives ST-ependymoma formation from periventricular neural stem cells in mice and that *RELA^FUS^*-induced tumorigenesis is likely dependent on a series of cell signaling pathways in addition to NF-κB.

INTRODUCTION

Ependymomas account for 10% of intracranial tumors in children and 4% of brain and spinal cord tumors in adults (Chamberlain, 2003; Rudà et al., 2008). Genomic studies have subdivided supratentorial (ST), posterior fossa (PF) and spinal (SP) ependymomas into clinically meaningful and molecularly distinct subgroups (Johnson et al., 2010; Mack et al., 2014; Pajtler et al., 2015; Parker et al., 2014; Taylor et al., 2005; Witt et al., 2011). Despite these insights, all ependymomas are similarly treated with surgery and radiotherapy. Chemotherapy is not used

routinely to treat ependymoma because it is largely ineffective (Bouffet and Foreman, 1999; Merchant et al., 2009).

Recent next-generation sequencing studies have discovered recurrent chromosomal translocations in a subset of ST-ependymomas that generate distinct fusion oncogenes (Parker et al., 2014). Seventy-two percent of ST-ependymomas contain *C11orf95-RELA* fusions (Pajtler et al., 2015; Parker et al., 2014). Patients with these tumors have a 5-year progression-free survival of <30% (hereafter termed the ST-ependymoma [EPN]-RELA subtype). A further 10% of ST-ependymomas contain either *C11orf95-YAP1*, *YAP1-MAMLD1*, or *YAP1-FAM118B* fusions (ST-EPN-YAP1 subtype) and have a much better 5-year progression-free survival of 66% (Pajtler et al., 2015; Parker et al., 2014). *RELA* and *YAP1* fusions are highly restricted to ST-ependymomas, supporting the notion that regional neural cell types are uniquely susceptible to specific genetic mutations (Johnson et al., 2010; Mohankumar et al., 2015; Taylor et al., 2005). The remaining 18% of ST-ependymomas are subependymomas that lack fusion genes and have an excellent clinical outcome (Pajtler et al., 2015; Parker et al., 2014).

We showed recently that the two most common *C11orf95-RELA* fusions (*RELA^FUS1^* and *RELA^FUS2^*) and *C11orf95-YAP1* (but not *C11orf95*, *RELA*, or *YAP1* alone) can transform embryonic mouse neural stem cells *ex vivo* (Parker et al., 2014). Although expression of *RELA^FUS1^* was shown to activate nuclear factor κB (NF-κB) signaling, whether this is required for transformation and whether fusions can drive ependymomagenesis *de novo* in the brain is not known. To test this, we used the RCAS/tv-a system to deliver the *RELA^FUS1^* fusion or fusion variants engineered to contain mutations in critical portions of RELA to Nestin-, glial fibrillary acidic protein (GFAP)-, or BLBP-expressing cells in the mouse brain. Neither *C11orf95* nor *RELA* alone were sufficient to drive tumorigenesis. Expression of
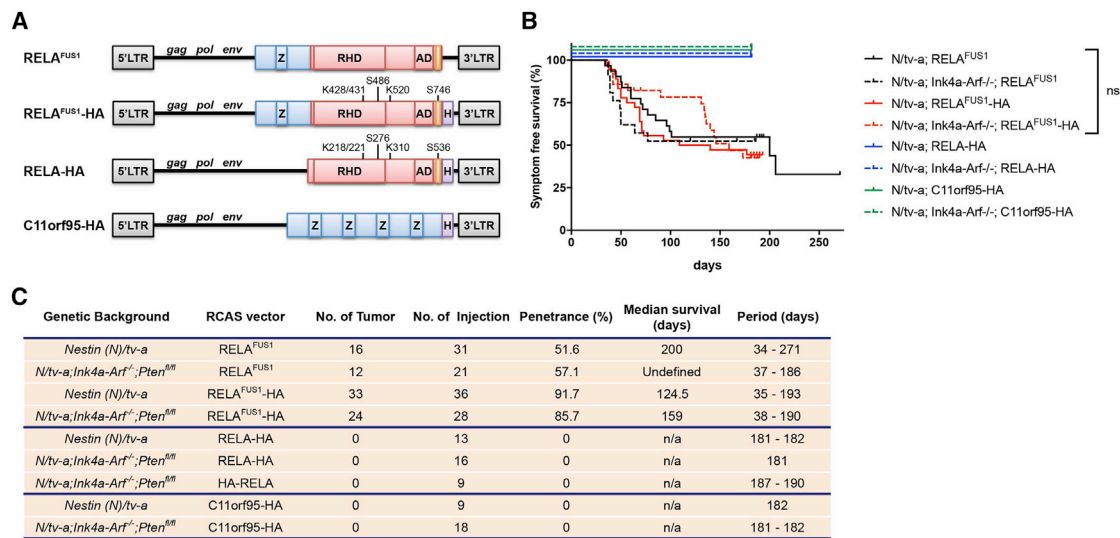
Figure 1. Somatic Cell Gene Transfer of C11orf95-RELA into Nestin-Expressing Cells Drives Brain Tumorigenesis

(A) Schematic of various RCAS vectors. Blue and red boxes represent components of *C11orf95* and *RELA* coding sequences, respectively. Z, zinc finger (C2H2-like); RHD, Rel homology domain; AD, activation domain; orange box, 9aaTAD; H, HA tag. The phosphorylation and acetylation sites of the *RELA^FUS1* gene product corresponding to those of RELA are also described.

(B) Kaplan-Meier survival curves showing symptom-free survival of RCAS-*RELA^FUS1* (black line) and *RELA^FUS1*-HA (red line), RELA-HA (blue line), or *C11orf95*-HA (green line) injection in *Nestin (N)/tv-a* (regular line) or *N/tv-a;Ink4a-Arf^{-/-}* (dotted line) mice. Tumor formation was observed by injection of these RCAS viruses into neonatal pups brains. n.s., not significant.

(C) Summary of the RCAS vector injections in *N/tv-a* or *N/tv-a;Ink4a-Arf^{-/-}* mice.

RELA^FUS1 in our system upregulated a broad array of genes that included an NF-κB-associated transcriptional signature; however, *RELA^FUS1* mutants with selective mutation of the Rel homology domain (RHD) as well as constitutively active RELA mutants failed to induce brain tumor formation. The data suggest that *RELA^FUS1* is adequate to drive EPN formation *de novo* in the brain. The oncogenic effect of *RELA^FUS1* requires the Ser 486, but not Ser 746, phosphorylation site in the fusion protein and produces biologic effects that are not restricted to NF-κB.

RESULTS

### *C11orf95-RELA* Drives Brain Tumorigenesis

RELA^FUS1 accounts for almost half of all *C11orf95-RELA* fusions and includes the N-terminal portion of *C11orf95* and all but the first two codons of *RELA* (Parker et al., 2014). To test the ability of *RELA^FUS1* to form ependymomas *de novo*, we used the RCAS/tv-a system to express *RELA^FUS1* in specific brain cell types in mice (Holland et al., 1998; Holland and Varmus, 1998). *RCAS-RELA^FUS1* or *RCAS-RELA^FUS1-HA* (containing a C-terminal human influenza hemagglutinin [HA] tag) were first expressed in Nestin-expressing brain cells using *Nestin (N)/tv-a* mice (Figures 1A and S1; Holland et al., 1998). Fifty-two percent and 92% of mice injected with *RCAS-RELA^FUS1* or *RCAS-RELA^FUS1-HA*, respectively, but not a control, developed tumors within 2 months of injection (Figures 1A–1C; Table S1A). In stark contrast, *RCAS-HA-RELA*, *RCAS-RELA-HA*, or *RCAS-C11orf95-HA* failed to generate tumors, confirming our prior observations that *RELA^FUS1*, but neither translocation partner gene alone, is competent to drive tumorigenesis (Figures 1A–1C and S1; Parker

et al., 2014). Notably, although *CDKN2A* (*INK4A-ARF*) is deleted in some ST-EPN-RELA tumors and enhances platelet-derived growth factor (PDGF)-induced glioma formation in mice, *RELA^FUS1*-induced tumorigenesis neither required, nor was it accelerated by, *Ink4a-Arf* deletion in mice (Figures 1B and 1C; Table S1B; Fomchenko et al., 2011; Ozawa et al., 2014; Pajtler et al., 2015).

RELA^FUS1-Induced Mouse Tumors Recapitulate ST-EPN Histology

RELA^FUS1-induced tumors were well circumscribed, predominantly intra-ventricular tumors that displayed several histological features characteristic of ependymoma, including a biphasic architectural pattern of dense cell clusters alternating with hypocellular regions and relatively little necrosis (Figures 2A and S2A) but no canonical ependymal rosettes and pseudorosettes, although similar structures were sometimes observed (Figure 2B). *RELA^FUS1*-induced tumors also contained a network of delicate branching capillaries similar to that observed in our *ex vivo RELA^FUS1*-induced tumor model (Parker et al., 2014) and the vascular variant of human ST-ependymomas (Figure 2B; Figarella-Branger et al., 2016; Godfraind et al., 2012; Rousseau et al., 2007). These morphological findings were obviously distinct from both astrocytic and oligodendrocytic glioma mouse models and human glioblastoma (GBM) presenting an infiltrative growth pattern and glomeruloid microvascular formation (Figures 2A and 2B and S2B–S2F). Immunostaining and electron microscopy of *RELA^FUS1*-induced tumors identified additional features common to human ependymomas, including expression of GFAP and Olig2 and interdigitating tumor cell processes (Figures
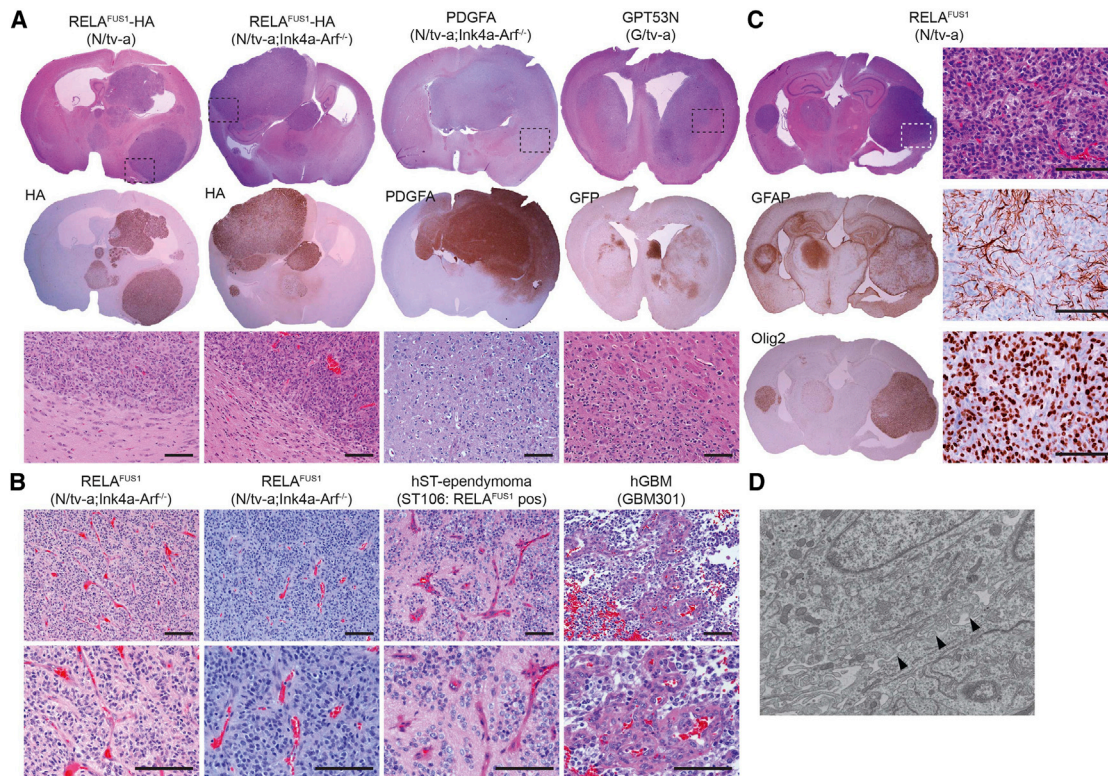
Figure 2. RELA^FUS1^-Induced Mouse Tumors Recapitulate Human ST-EPN Histology

(A) Representative H&E and immunohistochemistry (IHC) images of RCAS-*RELA^FUS1^-HA-*, *PDGFA-*, and *GPT53N-*induced brain tumors in the indicated *tv-a* mice. HA, PDGFA, and GFP antibody immunoexpression represents essentially the vector expression. Dashed boxes at the top denote the enlarged regions as shown at the bottom. Scale bars, 100 μm.

(B) Representative H&E stainings of *RELA^FUS1^-*induced brain tumors in *N/tv-a;Ink4a-Arf*^−/−^ mice, human *RELA^FUS1^-*positive ST-ependymoma, and human GBM. Scale bars, 100 μm.

(C) Representative H&E and IHC analysis with the indicated antibodies of RCAS-*RELA^FUS1^-*induced brain tumors in *N/tv-a* mice. All enlarged images represent the areas of dashed boxes in H&E staining. Scale bars, 100 μm.

(D) Representative ultra-structure of a *RELA^FUS1^-*induced brain tumor. Black arrowheads show interdigitating tumor cell processes.

2C and 2D and S2E and S2F; Liberski, 1996; Otero et al., 2011). Furthermore, we showed previously that human ST-EPN-RELA tumors display intense nuclear RELA immunoreactivity (Parker et al., 2014). The same immunohistochemical feature was displayed by our *de novo RELA^FUS1^-*induced tumors but not by similarly generated *PDGFA-* or *shNf1* (*GPT53N*)-driven mouse gliomas (Figure 3A). These observations were further validated in a cohort of human ST- (n = 23), PF- (n = 49), and SP-ependymomas (n = 48) and GBMs (n = 30) (Figures 3B and 3C and S3A–S3E; Tables S2A–S2C). Thus, our *RELA^FUS1^-*induced brain tumors recapitulate the principal growth, morphological, and immunohistochemical features of human ST-EPN-RELA tumors.

*RELA^FUS1^*-Induced Mouse Tumors Express a Human ST-EPN-RELA-like Transcriptome

To further assess the fidelity of the *RELA^FUS1^-*EPN mouse model, we performed RNA sequencing (RNA-seq) analysis of these tumors and compared their transcriptomes with those of normal mouse brain and *PDGFA-*driven mouse gliomas (Table S3). Principal-component analysis clearly segregated *RELA^FUS1^-*ependymoma, *PDGFA-*driven glioma, and normal brain tran-

scriptomes, confirming the distinct biologies of these tissues (Figure 4A). Next, to test whether *RELA^FUS1^-*driven mouse transcriptomes recapitulate those of human ST-EPN-RELA, we compared their transcriptomes using cross-species gene set enrichment analysis (GSEA) (Supplemental Experimental Procedures). Gene sets that define human ST-ependymoma, and in particular ST-EPN-RELA, but not human PF- or SP-ependymoma, were significantly enriched in mouse *RELA^FUS1^-*driven tumor transcriptomes (Figures 4B–4E; Pajtler et al., 2015; Taylor et al., 2005). Thus, in addition to displaying the morphologic and immunophenotypic characteristics of ST-EPN-RELA, *RELA^FUS1^-*ependymomas also recapitulate the transcriptome of human ST-EPN-RELA.

We showed previously that RELA^FUS1^ translocates spontaneously to the nucleus of mouse neural stem cells to activate the transcription of a large number of genes, including NF-κB target genes (Parker et al., 2014). In keeping with these data, genes that were significantly upregulated in *de novo RELA^FUS1^-*induced mouse ependymomas relative to normal brain included 52% (n = 158 of 302) of validated NF-κB target genes (false discovery rate [FDR] p = 4.7×10^{-7}), and GSEA identified
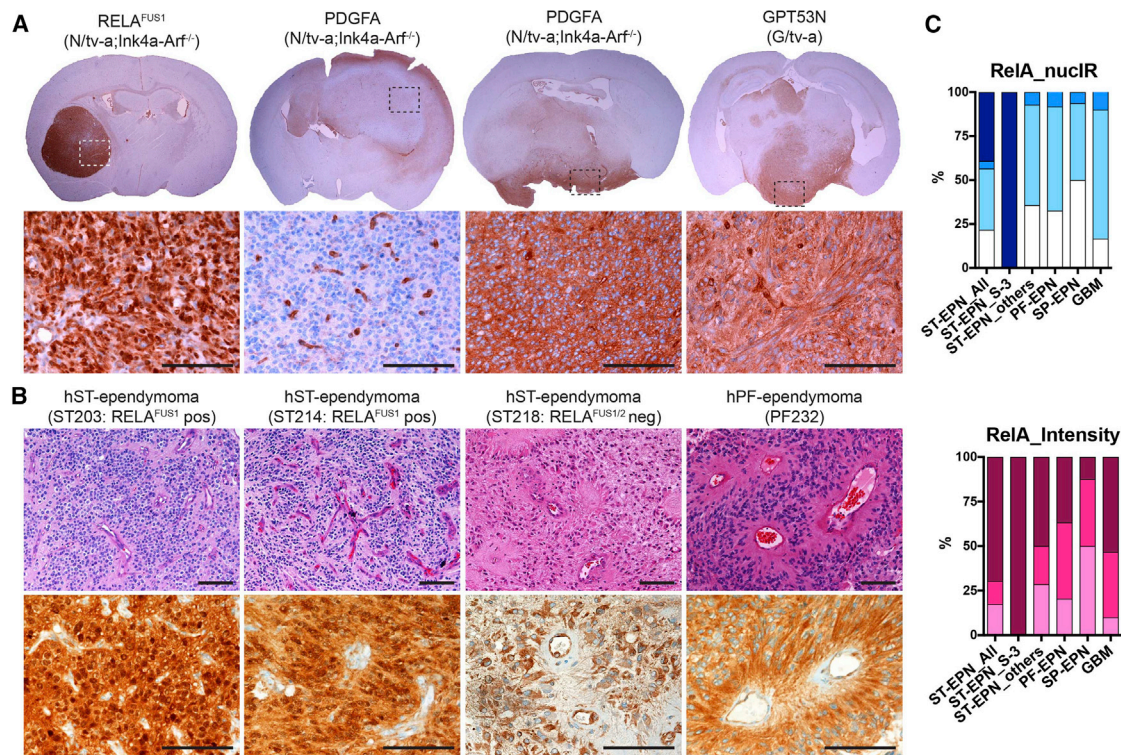
Figure 3. RELA Expression in Mouse and Human RELA^FUS1 EPNs

(A) Representative IHC analysis for RELA of RCAS-*RELA^FUS1*-, *PDGFA*-, and *GPT53N*-induced brain tumors in the indicated *tv-a* mice. Dashed boxes at the top denote the enlarged regions as shown at the bottom. Scale bars, 100 μm.

(B) Representative H&E and IHC analysis for RELA of human *RELA^FUS1*-positive (ST203, ST214) and RELA^FUS1/2^-negative (ST218) ST-ependymomas and PF-EPN (PF232). All IHC images show the same area as each H&E images. Scale bars, 100 μm.

(C) Summary of semiquantitative immunohistochemical analysis for RELA in human ependymomas and GBMs. The immunoexpression level was evaluated using two criteria: nuclear immunoreactivity (NucIR) and staining intensity as described in Figure S3D and Table S2B.

See also Supplemental Experimental Procedures.

"TNFA_signaling_via_NFKB" as one of the most enriched gene sets in these tumors (FDR, q value 6.39×10^{-43}). Furthermore, hierarchical clustering using validated NF-κB target genes alone readily segregated *de novo* mouse *RELA^FUS1*-EPN (EP), *PDGFA*-driven glioma (GM) and normal mouse brain (NB) transcriptomes (Figure 4F). Thus, RELA^FUS1 activates NF-κB target gene transcription following *de novo* tumor formation *in vivo* as well as in neural stem cells *in vitro*.

RELA^FUS1 Induces an Aberrant Non-Canonical NF-κB Transcriptional Cassette

Although overexpression of wild-type *RELA* in neural stem cells activates gene transcription, this is restricted to NF-κB target genes and does not promote malignant transformation (Figures 1B and 1C; Tables S1A–S1D; Parker et al., 2014). Thus, aberrant NF-κB signaling appears to be associated with, but not sufficient, to drive *RELA^FUS1*-induced tumorigenesis. Therefore, to better understand how *RELA^FUS1* drives transformation, we looked for non-NF-κB target genes that were dysregulated in both our *ex vivo* and *de novo* RELA^FUS1-induced mouse ependymomas. Nine thousand nine hundred and sixty-five genes were significantly up- or downregulated in either our *ex vivo* neural stem

cell (Parker et al., 2014) or *de novo RELA^FUS1*-induced mouse brain tumors relative to mouse normal neural stem cells and brain, respectively (p < 0.05 FDR). A significant number of these genes was commonly dysregulated in both tumors, including 13% that were upregulated (n = 1,271 of 9,965) and 4% that were downregulated (n = 400 of 9,965) in both tumor models (p = 2.3×10^{-6} for overlap) (Table S4). Only 6% of these genes (n = 102 upregulated, n = 1 downregulated) are known NF-κB targets (Table S4A). GSEA segregated the remaining 1,568 "non-NF-κB" target genes into nine broad classes (Table S4B). Remarkably, we showed previously that six of these classes are dysregulated when mouse neural stem cells are transformed by non-fusion EPN oncogenes (Mohankumar et al., 2015). These included negative enrichment of synaptogenesis and vesicle trafficking regulators (e.g., INTRACELLULAR_VESICLE, n = 137 of 1,259, FDR q value = 2.84×10^{-51}), consistent with our observation that these genes are selectively deleted during ST-EPN tumorigenesis (Mohankumar et al., 2015). The five other gene classes commonly enriched with those in non-RELA^FUS1 EPN included stem cell function and neuronal differentiation (e.g., REGULATION_OF_CELL_DIFFERENTIATION, n = 160 of 1,492, FDR q value = 3.20×10^{-59}), immunity and inflammation
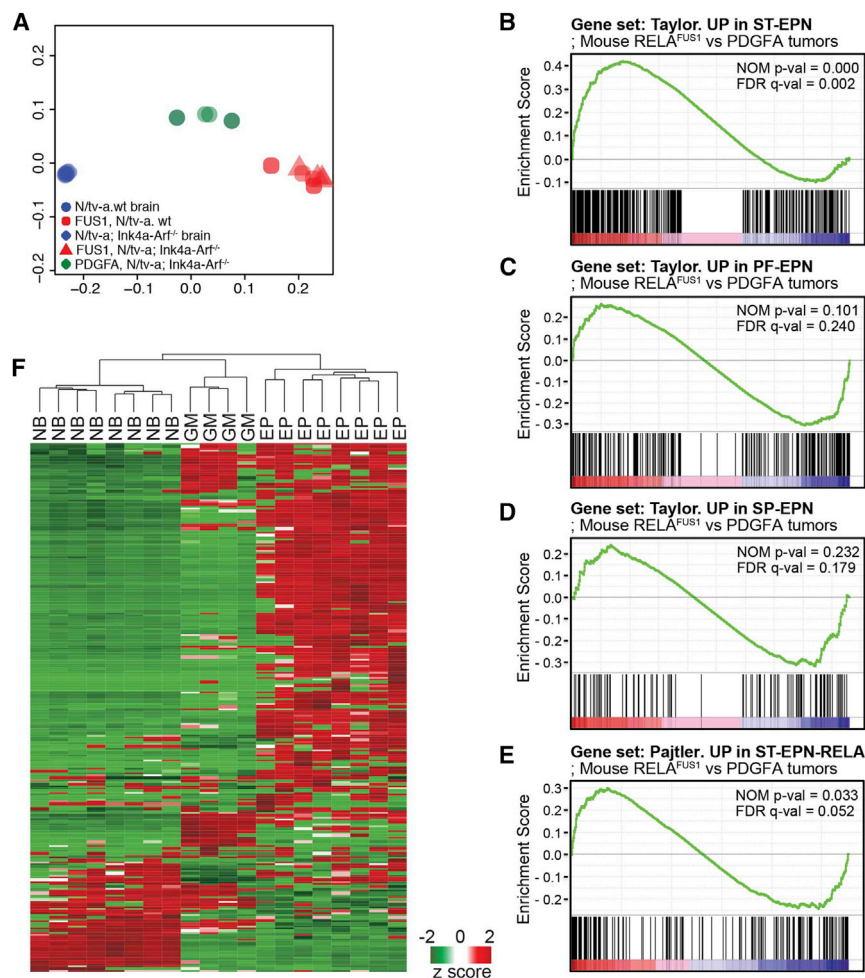
Figure 4. RELA^FUS1-Induced Mouse Tumors Express a Human ST-EPN-RELA-like Transcriptome

(A) Principal-component analysis with gene expression profiling of *RELA^FUS1* ependymomas, *PDGFA*-driven murine gliomas, and normal mouse brains.

(B–E) Gene set enrichment analysis (GSEA) of *RELA^FUS1* ependymomas and *PDGFA*-induced gliomas. Gene expression profiles were compared between both mouse tumor types using gene sets based on ST- (B), PF- (C), and SP-EPN (D) or ST-EPN-RELA's (E) gene expression signatures (Pajtler et al., 2015; Taylor et al., 2005). The nominal p value (NOM p-val) and false discovery rate (FDR)-corrected q value (FDR q-val) are indicated. A nominal p value of <0.05 was considered significant in this analysis.

(F) Unsupervised hierarchical cluster analysis of 302 validated NF-κB target genes expressed *de novo* in mouse *RELA^FUS1*-EPN (EP), *PDGFA*-driven glioma (GM), and normal mouse brain (NB) (http://www.bu.edu/nf-kb/gene-resources/target-genes/; T. D. Gilmore; Parker et al., 2014).

(e.g., REGULATION_OF_CYTOKINE_PRODUCTION, n = 114 of 563, FDR q value = 8.71×10^{-69}), the epigenome (SILENCED_BY_METHYLATION, n = 67 of 282, FDR q value = 6.14×10^{-47}), and those associated with other cancer types. Notably, this latter class included positive enrichment of genes associated with the mesenchymal subtype of glioblastoma (GLIOBLASTOMA_MESENCHYMA, n = 95 of 216, FDR q value = 2.26×10^{-95}). By addition to these six broad classes, *RELA^FUS1*-induced transformation also enriched the expression of genes controlling cell-cell adhesion (e.g., BIOLOGICAL_ADHESION, n = 155 of 1,032, FDR q value = 4.27×10^{-75}) and downregulated genes controlling the transmembrane transport of ions (e.g., ION_TRANSPORT, n = 45 of 1,262, FDR q value = 1.23×10^{-12}) that we did not observe during the formation of non-RELA^FUS1 EPN (Mohankumar et al., 2015). Together, these data suggest that all forms of ST-ependymomagenesis require dysregulation of synaptogenesis and vesicle trafficking, stem cell function and neuronal differentiation, immunity and inflammation, the epigenome, and functions associated with other cancer types; however, dysregulation of cell-cell adhesion and ion transport might be associated more selectively with *RELA^FUS1*-induced transformation.

Because loss of *Ink4a-Arf* did not affect the tumor latency of our RELA^FUS1-induced ependymomas, we investigated the dysregulation of alternative pathways. Accumulation of TP53 is very frequent in human ST-EPN-RELA tumors and associated with a poor prognosis, although this gene mutation is rare (Tzaridis et al., 2016). Furthermore, the accumulated TP53 is thought to be functionally impaired in ependymomas (Gaspar et al., 2006; Tzaridis et al., 2016; Verstegen et al., 2002). Therefore, we focused on Trp53 status in the mouse tumors. Consistent with frequent accumulation of TP53 in human *RELA^FUS*-positive cases (Tzaridis et al., 2016), evident upregulation of the Trp53 pathway and elevated *Trp53* mRNA expression were observed in *RELA^FUS1*-induced tumors in both N/tv-a and N/tv-a; *Ink4a-Arf^{−/−}* mice (Figures S4A–S4). Thus, it is possible that the effect of *Ink4a-Arf* loss in *RELA^FUS1*-induced EPN formation was blurred by dysregulation of the TP53 pathway in our model, leading to no survival difference between the genetic backgrounds (Figures 1B and 1C).

Serine-486 of RELA^FUS1 (Corresponding to Serine-276 of RELA) Is Critical to Drive Tumorigenesis

The aberrant juxtaposition of genes within fusion proteins following chromosomal translocation may result in the uncontrolled activation of fusion partners or the acquisition of novel functions (Mertens et al., 2015). Our transcriptomic analyses of *RELA^FUS1*-driven tumors suggest that this fusion activates NF-κB signaling and a series of other cell pathways. Therefore, to further dissect the NF-κB- and non-NF-κB-related transforming functions of RELA^FUS1, we created a series of mutant forms of wild-type *RELA* and *RELA^FUS1* and tested the capacity
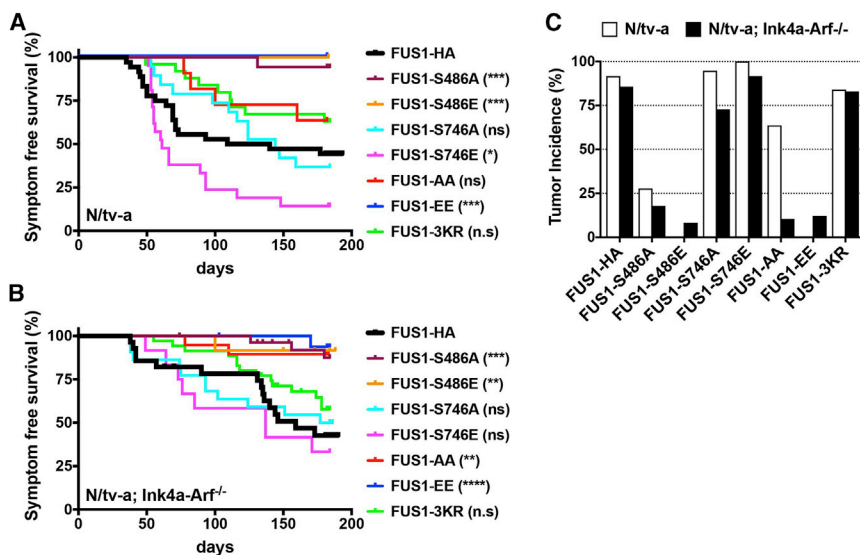
Figure 5. Serine-486 of RELA^FUS1^ Is Critical to Drive Tumorigenesis

(A and B) Kaplan-Meier survival curves showing symptom-free survival of *RELA^FUS1^-HA* or *RELA^FUS1^-HA* mutant-induced brain tumors in *N/tv-a* (A) and *N/tv-a; Ink4a-Arf^−/−* (B) mice. The survival curves of the *RELA^FUS1^-HA*-induced tumors from Figure 1B are also shown for comparison. Statistical comparison of each mutant with *RELA^FUS1^-HA* is also shown in the legends and Table S1C. *p < 0.05, **p < 0.01, ***p < 0.001, ****p < 0.0001.

(C) Tumor incidence of RELA-HA, RELA^FUS1^-HA, or the relevant mutant injection in *N/tv-a* and *N/tv-a;Ink4a-Arf^−/−* mice.

See also Tables S1A–S1C.

of these constructs to drive tumorigenesis in our RCAS/tv-a system *in vivo*. Phosphorylation of Ser-276 and Ser-536 within the Rel homology and transactivation domains, respectively, has been reported to promote RELA transcriptional activity (Figure 1A; Chen and Greene, 2004; Hoesel and Schmid, 2013; Huang et al., 2010); however, introduction of phosphomimetic mutants of these residues (RELA-S276E, RELA-S536E, or combined RELA-S276E/S536E) into the brains of *N/tv-a* and *N/tv-a;Ink4a-arf^−/−* neonatal mice failed to drive tumorigenesis (Figures 1A and S5A; Tables S1A and S1B). Thus, consistent with our studies of overexpressed wild-type RELA (Parker et al., 2014), constitutively active RELA is not competent to drive ependymomagenesis.

We next created a series of *RELA^FUS1^* mutants and tested the ability of these to drive ependymomagenesis in the brains of *N/tv-a* and *N/tv-a;Ink4a-arf^−/−* neonatal mice (Figures 1A and S5B–S5D). A serine-glutamine substitution at Ser-486 of RELA^FUS1^ (corresponding to Ser-276 in the Rel homology domain of RELA) markedly reduced the transforming capacity of *RELA^FUS1^* (Figures 1A and 5A–5C; Tables S1A–S1C); RELA^FUS1^-S486E formed no tumors in 14 *N/tv-a* neonatal brains compared with a tumor penetrance of 92% (n = 33 of 36) in mice injected with RELA^FUS1^ (log ratio, p = 0.0009) (Figure 5C; Tables S1A and S1C). RELA^FUS1^-S486E-driven tumor penetrance was also much reduced in *N/tv-a;Ink4a-arf^−/−* neonatal mice (8%, n = 1 of 12) compared with 86% (n = 24 of 28) driven by RELA^FUS1^ (log ratio, p = 0.0095) (Figure 5C; Tables S1B and S1C). In contrast, a serine-glutamine substitution at Ser-746 (corresponding to Ser-536 of RELA) did not reduce tumorigenesis in either *N/tv-a* or *N/tv-a;Ink4a-arf^−/−* neonatal mice (Figures 1A and 5A–5C; Tables S1A–S1C). Constructs harboring both of these substitutions (RELA^FUS1^-S486E/S746E: EE) failed to drive tumorigenesis in the *N/tv-a* neonatal brain and drove tumors with a penetrance of only 12% (n = 4 of 33) in *N/tv-a;Ink4a-arf^−/−* neonatal mice (Figures 5A–5C; Tables S1A–S1C), suggesting that S486E had a negative effect on the brain tumor-forming capacity of RELA^FUS1^. Two additional constructs carrying serine-alanine substitutions at these

same residues (RELA^FUS1^-S486A and RELA^FUS1^-S486A/S746A: AA) also abolished and markedly reduced RELA^FUS1^-driven ependymomagenesis in *N/tv-a* (S486A, log rank test, p = 0.0006; S486A/S746A, log rank test, p = 0.1731) and *N/tv-a; Ink4a-arf^−/−* (S486A, log-rank test, p = 0.0004; S486A/S746A, log-rank test, p = 0.0024) neonatal mouse brains, respectively (Figures 5A–5C; Tables S1A–S1C), whereas RELA^FUS1^-S746A did not affect tumorigenesis. Thus, Ser-486, but not Ser-746, appears to be critical for *RELA^FUS1^*-driven ependymomagenesis.

Acetylation of RELA has also been reported to regulate NF-κB activity (Huang et al., 2010). Acetylation of lysine-310 (K310) has been reported to promote full transcriptional activity (Chen et al., 2002; Huang et al., 2010), and K221/K218 acetylation enhances DNA binding and prevents nuclear export. To test the importance of these residues in *RELA^FUS1^*-driven tumorigenesis, we generated lysine-to-arginine unacetylatable mutants in the residues corresponding to K218, K221, and K310R of RELA (RELA^FUS1^-K428R/K431R/K520R: 3KR; Figures 1A, S5B, and S5E; Chen et al., 2002). RELA^FUS1^-3KR drove ependymomas with high penetrance in *N/tv-a* (84%, n = 21/25) and *N/tv-a; Ink4a-Arf^−/−* (83%, n = 29 of 35) mice, indicating that acetylation of these residues is dispensable for *RELA^FUS1^*-driven tumorigenesis (Figures 5A-5C; Tables S1A–S1C).

Disruption of Cell-Cell Adhesion Is a Critical Component of RELA^FUS1^-Driven Tumorigenesis

We reasoned that comparing the transcriptomes driven by *RELA^FUS1^* mutants that did or did not drive tumorigenesis might pinpoint cell functions that are critically associated with *RELA^FUS1^*-driven transformation. Multi-dimensional scaling (MDS) using NF-κB target genes as input (Tables S5 and S6) clearly segregated NIH 3T3/tv-a cells transduced with tumor-forming vectors (RELA^FUS1^, RELA^FUS1^-S746E, and RELA^FUS1^-3KR) from those transduced with non-transforming constructs (RELA-S276E, RELA^FUS1^-S486E, and RELA^FUS1^-EE), strongly suggesting that NF-κB activity is significantly associated with *RELA^FUS1^*-driven tumorigenesis (Figures 6A, S6A, and S6B). More than half of these genes were enriched for regulators of cell-cell adhesion and the extracellular matrix, immunity and inflammation, or vesicle
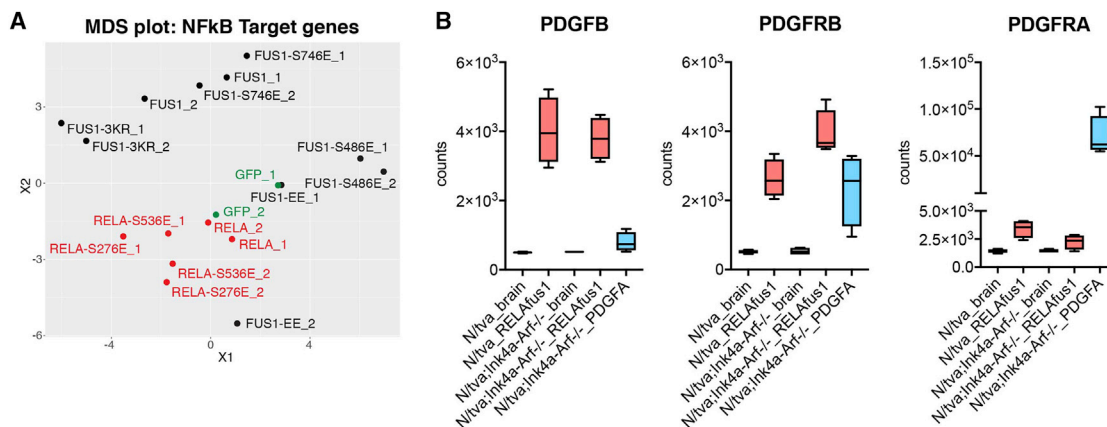
Figure 6. RNA-Seq Analysis of NIH3T3T Cells and RELA^FUS1^-Induced Mouse Tumors

(A) Multidimensional scaling (MDS) projection of sample similarities based on gene expression profiling analyzed with the NF-κB gene set in NIH 3T3T cells infecting the indicated RCAS vectors. See also Tables S5, S6, and S7.

(B) Boxplots of *PDGFB*, *PDGFRB*, and *PDGFRA* expression in mouse brain and brain tumor tissues. See also Table S3.

trafficking (Table S4B). Thus, RELA^FUS1^ might drive EPN tumorigenesis in part by dysregulating communication between tumor cells and the brain microenvironment, perhaps promoting local invasion and growth (Mohankumar et al., 2015).

Interestingly, in addition to these gene sets, both PDGF beta polypeptide (PDGFB) and its cognate receptor PDGF beta polypeptide (PDGFRB) were markedly upregulated in the transcriptomes of *RELA^FUS1^*-driven *ex vivo* and *de novo* ependymomas (Figure 6B; Parker et al., 2014) as well as selectively upregulated in those driven by tumorigenic RELA^FUS1^ mutants (Table S7). PDGFB is a highly potent neural oncogene (Dai et al., 2001); thus, *RELA^FUS1^* might also drive EPN tumorigenesis by upregulating oncogenic PDGFB-PDGFRB signaling.

The Normal Ventricular Wall as the Putative Location for Ependymomagenesis

Our prior cross-species analyses and *ex vivo* mouse modeling predict that neural stem cells in the lateral ventricular wall are cells of origin of EPN (Johnson et al., 2010; Mohankumar et al., 2015; Taylor et al., 2005). However, these studies involved cross-species mapping of human EPN gene expression profiles in normal developing mouse brain or *ex vivo* transduction of mouse neural stem cells that form tumors when reimplanted in the brain. Therefore, to better understand the origin of ependymoma, we took advantage of our *de novo RELA^FUS1^*-induced tumor model. These tumors were typically observed as intra- and/or peri-ventricular cerebral masses, although, rarely, tumors also occurred in the cerebral parenchyma not obviously connected with the ventricular system, similar to the growth pattern of human ependymomas (Figures 2A, 2C, 3A, S2A, and S7A–S7E). Histological analyses of early lesions developing within 31 days of RELA^FUS1^ injection into *N/tv-a* mice identified small lesions immediately adjacent to the ventricular system (Figures 7A and S7E).

To further understand the cellular origin of ependymoma, we tested the capacity of mice harboring different *tv-a* transgenes to develop *RELA^FUS1^*-driven ependymoma. *N/tv-a* used in the
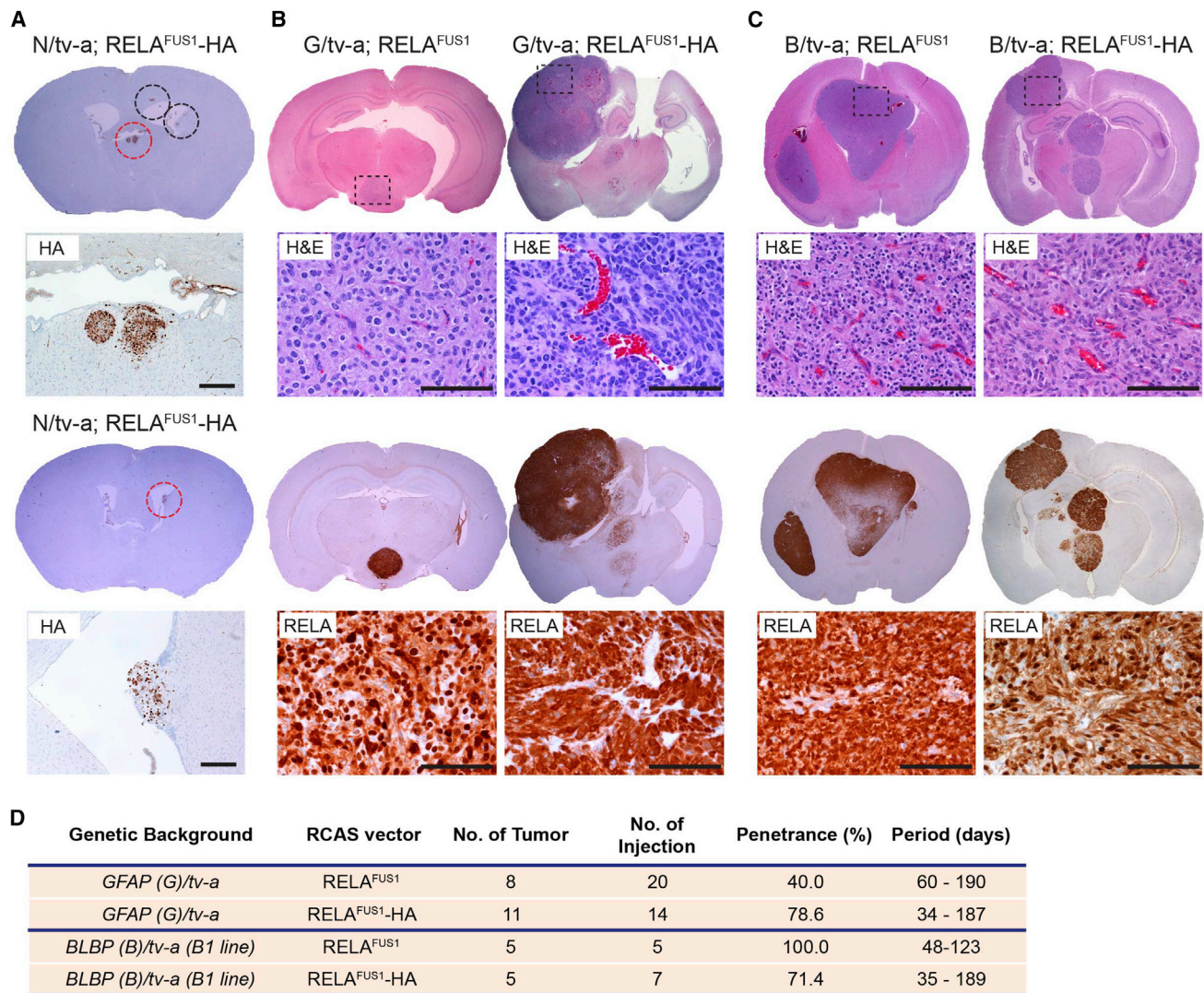
experiments described above specifically targets nestin-expressing neural stem and progenitor cells. Therefore, we investigated the oncogenic potential of the *RELA^FUS1^* gene in neonatal mouse brains when it is targeted to GFAP-expressing cells using *(G)/tv-a-* (Holland and Varmus, 1998) or BLBP (brain lipid binding protein, also known as fatty acid binding protein 7 or FABP7)-expressing cells using a *(B)/tv-a* transgenic mouse in which an expression of *tv-a*, a receptor for RCAS virus, was driven under a *GFAP* or *BLBP* promoter, respectively (Figures S7F–S7H). Tumors occurred in both of these transgenic lines with similar histologic features as those forming in the *N/tv-a* mice (or human ST-EPN) (Figures 7B and 7C; Table S1D). These data further support the notion that Nestin-, GFAP-, and BLBP-expressing neural stem and progenitor cells in the ventricular wall can serve as cells of origin of *RELA^FUS1^*-induced ST-ependymoma.

DISCUSSION

Unlike GBM with its multiple sequence and copy number alterations, the genome of human ST-EPN is relatively stable but contains a fusion gene that is sufficient to induce similar tumors in mice. Therefore, human ST-EPN may follow a single-hit oncogenesis model such as *BCR-ABL*-driven chronic myelogenous leukemia (CML) (Groffen et al., 1984). The oncogenic function of the *RELA* or *YAP1* fusion products in ST-EPN is not yet known, and it may or may not be easily targeted with small molecules. Genetically accurate mouse models of this disease will certainly help with the development of such therapies should they become available.

The location of the cell of origin of *RELA^FUS1^*-EPN in the mouse seem to be at the edge of the subventricular zone (SVZ), consistent with what one might imagine for human ST-ependymoma. At this point, it is not clear whether the oncogenic function of this fusion protein occurs in the nucleus or cytoplasm. When it comes to the driving functions of the *RELA* fusion products, RELA^FUS1^ does have NF-κB activity, but it is worth noting that neither the individual components of or activated versions of RELA form

A N/tv-a; RELA^FUS1-HA

B G/tv-a; RELA^FUS1 · G/tv-a; RELA^FUS1-HA

C B/tv-a; RELA^FUS1 · B/tv-a; RELA^FUS1-HA

D

Genetic Background	RCAS vector	No. of Tumor	No. of Injection	Penetrance (%)	Period (days)
GFAP (G)/tv-a	RELA^FUS1	8	20	40.0	60 - 190
GFAP (G)/tv-a	RELA^FUS1-HA	11	14	78.6	34 - 187
BLBP (B)/tv-a (B1 line)	RELA^FUS1	5	5	100.0	48-123
BLBP (B)/tv-a (B1 line)	RELA^FUS1-HA	5	7	71.4	35 - 189

Figure 7. The Normal Ventricular Wall as the Putative Location for Ependymomagenesis
(A) Representative IHC images of the HA tag of RCAS-*RELA^FUS1-HA*-induced brain tumors in *N/tv-a* mice (see also Figure S7E). Brain tumor formation was examined with HA tag staining 1 month post-injection. Dashed circles at the top show early lesions representing, essentially, RCAS vector expression. Red dashed circles denote the enlarged regions as shown at the bottom. Scale bars, 200 μm.
(B and C) Representative H&E and IHC images for RELA of *RELA^FUS1* or *RELA^FUS1-HA*-induced brain tumors in *GFAP(G)/tv-a* (B) or *BLBP(B)/tv-a* mice (C). Enlarged areas for H&E and RELA are shown as a dashed box in each H&E brain. Scale bars, 100 μm.
(D) Summary of RCAS-*RELA^FUS1* or *RELA^FUS1-HA* vector injections in *G/tv-a* or *B/tv-a* mice.

ependymomas. Several lines of evidence suggest that the oncogenic driving functions of *RELA* fusion products may be more than aberrant NF-κB activity. We found that RELA^FUS1 drives several other biological processes, including vesicular transport, development of cytokine production, and cell-cell adhesion. The importance of cell-cell adhesion in the oncogenic effect of RELA^FUS1 is further underscored by a series of mutant forms of *RELA^FUS1*, where expression programs affecting cell-cell adhesion specifically characterize mutants of this fusion oncogene. Further, only a subset of residues critical for RELA activity are essential for oncogenic activity of RELA^FUS1. Finally, the amount of PDGF and its receptor induced by RELA^FUS1 in murine ST-

EPN are comparable with the amounts of these proteins sufficient to drive oncogenesis in RCAS/tv-a mouse models of gliomas. It therefore seems possible that at least part of the oncogenic effect of RELA^FUS1 in the CNS includes induction of PDGF signaling.

Our model faithfully recapitulated the histologic features and molecular profile of human *RELA* fusion-positive ependymomas. However, given that *RELA* fusions were generated by a chromothripsis event on chromosome 11, the gene rearrangement might affect the status of other genes on the chromosome with various degrees. Therefore, although *RELA* fusion alone is sufficient to form brain tumors in mice, the molecular mechanism underlying

RELA fusion driven-tumorigenesis in humans could be more complex and influenced by other altered neighboring genes.

The emerging data regarding this tumor type provides the potential for diagnostic tests that clearly distinguish these tumors from other glial neoplasms. Immunohistochemical analysis of tumors revealed strong nuclear-localized RELA staining in the *RELA*[FUS]-positive EPN and less nuclear or even nuclear-excluded RELA staining in the case of other ependymomas and gliomas. Obviously a more direct measure of the presence of *RELA*[FUS] would be RT-PCR for the various possible mRNAs encoding these fusion proteins. Of course, creating such a set of diagnostic tools would be much more compelling when a therapeutic strategy aimed at the *RELA*[FUS1] gene product has been developed.

EXPERIMENTAL PROCEDURES

Human Tumor Samples and Patient Characteristics
Formalin-fixed paraffin-embedded (FFPE) human EPN samples (n = 120) were obtained from the Department of Pathology at the University of Washington (UW; Seattle, WA; n = 56), Kitasato University (Kanagawa, Japan; n = 51), and Kanazawa University (Kanazawa, Japan; n = 13). In addition, 30 samples of surgically resected World Health Organization (WHO) grade IV GBMs were retrieved from the University of Washington pathology archive and were utilized as control groups. These samples were diagnosed according to the WHO classification (Louis et al., 2016) and had IRB (institutional review board) approval at each institution (University of Washington; IR File 8305; Kanazawa University, 2015-010 [396]; Kitasato University, B13-191). Clinical and pathologic characteristics are summarized in Table S2A. Recurrent ependymomas were categorized in primary sites regardless of the recurrent location in this study. Several available frozen samples from Kitasato University were also used for RT-PCR detection of *RELA*[FUS1] and *RELA*[FUS2].

Generation of Murine Brain Tumors
All animal experiments were done in accordance with protocols approved by the Institutional Animal Care and Use Committees of Fred Hutchinson Cancer Research Center (FHCRC) and followed NIH guidelines for animal welfare. The RCAS/tv-a system used in this work has been described previously (Holland et al., 1998, 2000; Holland and Varmus, 1998; Ozawa et al., 2014). *GFAP (G)/tv-a*, *Nestin (N)/tv-a* (agouti), *N/tv-a;Ink4a-Arf*^{−/−};*Pten*^{fl/fl}, or *BLBP (B)/tv-a* mice were used for RCAS-mediated brain tumor formation in this study. Briefly, DF-1 cells were transfected with the indicated RCAS plasmid using X-tremeGENE 9 DNA transfection reagent (Roche) according to the manufacturer's protocol. After checking RCAS expression with western blotting analysis, the cells (1 μL of 1×10^5 cells) were injected into newborn pup brains (within 3 days after birth). The mice were monitored until they developed symptoms of disease, such as lethargy, poor grooming, weight loss, dehydration, macrocephaly, seizures, jumping, and paralysis, or until 6 months after injection. Cases that failed to wean due to severe hydrocephalus caused by injection trauma and an inflammatory response against DF-1 cells were excluded from this study. Mouse brains were then used for subsequent analyses such as survival analysis, immunohistochemistry, and RNA-seq. Kaplan-Meier analysis demonstrating symptom-free survival of murine brain tumors was performed using log rank test in the Prism 7 software (GraphPad) for all mice injected with the relevant RCAS virus. Log rank p values were measured with the Mantel-Cox test. A value of p < 0.05 was considered significant in this study.

H&E Staining and Immunohistochemistry
Mouse brains were paraffin-embedded, sectioned, and stained with H&E as described previously (Hambardzumyan et al., 2009; Holland et al., 2000). Immunohistochemical staining of mouse brains and human specimens was performed with an automated staining processor using the Discovery DAB Map Detection Kit according to standard protocols as described previously (Ventana Medical Systems, Tucson, AZ) (Hambardzumyan et al., 2008). For ambiguous cases, the staining was repeated and carefully examined. Human ST-ependymomas were stained at least twice. See also Supplemental Experimental Procedures.

Plasmids
All vectors used in this study are listed in Table S1E. The details of vector constructs are described in the Supplemental Experimental Procedures.

Western Blot Analysis
Cells were cultured, lysed, and processed for western blotting by standard methods. See also Supplemental Experimental Procedures.

RNA-Seq Analysis for Murine Brain Tumors and NIH 3T3T Cells
Tumor tissues and half normal forebrains were macroscopically dissected and quickly crushed in liquid nitrogen. Total RNAs for mouse tissues and NIH 3T3T cells were extracted with the RNeasy Mini Kit (QIAGEN) according to the manufacturer's protocol and then labeled and amplified with the Illumina protocol, followed by sequencing on Illumina HiSeq2500 at the Genomics Shared Resource at FHCRC. RNA-seq reads were aligned to the University of California, Santa Cruz (UCSC) mm10 assembly using Tophat2 (Kim et al., 2013) and counted for gene associations against the UCSC genes database with HTSeq. Batch effects were corrected using the R function combat from the R package swamp (https://cran.r-project.org/web/packages/swamp/index.html). Log2 normalized data were used for subsequent principal-component analysis, MDS, and GSEA in R. Differential expression analysis was performed using the R/Bioconductor package limma (Ritchie et al., 2015). See also Supplemental Experimental Procedures.

DATA AND SOFTWARE AVAILABILITY

The accession numbers for the raw sequencing data and read count per gene data reported in this paper are SRA: SRP096964 and GEO: GSE93765, respectively. All codes in this study are available upon request.

SUPPLEMENTAL INFORMATION

Supplemental Information includes Supplemental Experimental Procedures, seven figures, and seven tables and can be found with this article online at https://doi.org/10.1016/j.celrep.2018.04.099.

ACKNOWLEDGMENTS

AUTHOR CONTRIBUTIONS

T.O. was involved in all aspects of the experiments and data analysis. G.J.-S. designed the immunohistochemical analysis, performed the experiments and

data analysis, and analyzed clinical information of human samples. S.A. and H.B. analyzed RNA-seq data. F.S. and R.K. were involved in RNA-seq analysis and contributed to preparation of the manuscript. Y.M., Y.Y., M.N., and T.K. collected clinical samples and analyzed the clinical information. J.B. contributed to the data analysis of immunohistochemistry and clinical sample information. J.D. and D.W.E. performed immunohistochemistry, iFISH, and electron microscopic analysis and pathological examination of mouse and human samples. T.S.J. provided reagents and contributed to vector construction. D.W.E. and R.J.G. provided critical insights into the study. T.O., R.J.G., and E.C.H. conceived the study and wrote the manuscript. R.J.G. and E.C.H. coordinated and supervised the study.

REFERENCES

Bouffet, E., and Foreman, N. (1999). Chemotherapy for intracranial ependymomas. Childs Nerv. Syst. *15*, 563–570.

Chamberlain, M.C. (2003). Ependymomas. Curr. Neurol. Neurosci. Rep. *3*, 193–199.

Chen, L.F., and Greene, W.C. (2004). Shaping the nuclear action of NF-kappaB. Nat. Rev. Mol. Cell Biol. *5*, 392–401.

Chen, L.F., Mu, Y., and Greene, W.C. (2002). Acetylation of RelA at discrete sites regulates distinct nuclear functions of NF-kappaB. EMBO J. *21*, 6539–6548.

Dai, C., Celestino, J.C., Okada, Y., Louis, D.N., Fuller, G.N., and Holland, E.C. (2001). PDGF autocrine stimulation dedifferentiates cultured astrocytes and induces oligodendrogliomas and oligoastrocytomas from neural progenitors and astrocytes in vivo. Genes Dev. *15*, 1913–1925.

Figarella-Branger, D., Lechapt-Zalcman, E., Tabouret, E., Jünger, S., de Paula, A.M., Bouvier, C., Colin, C., Jouvet, A., Forest, F., Andreiuolo, F., et al. (2016). Supratentorial clear cell ependymomas with branching capillaries demonstrate characteristic clinicopathological features and pathological activation of nuclear factor-kappaB signaling. Neuro-oncol. *18*, 919–927.

Fomchenko, E.I., Dougherty, J.D., Helmy, K.Y., Katz, A.M., Pietras, A., Brennan, C., Huse, J.T., Milosevic, A., and Holland, E.C. (2011). Recruited cells can become transformed and overtake PDGF-induced murine gliomas in vivo during tumor progression. PLoS ONE *6*, e20605.

Gaspar, N., Grill, J., Geoerger, B., Lellouch-Tubiana, A., Michalowski, M.B., and Vassal, G. (2006). p53 Pathway dysfunction in primary childhood ependymomas. Pediatr. Blood Cancer *46*, 604–613.

Godfraind, C., Kaczmarska, J.M., Kocak, M., Dalton, J., Wright, K.D., Sanford, R.A., Boop, F.A., Gajjar, A., Merchant, T.E., and Ellison, D.W. (2012). Distinct disease-risk groups in pediatric supratentorial and posterior fossa ependymomas. Acta Neuropathol. *124*, 247–257.

Groffen, J., Stephenson, J.R., Heisterkamp, N., de Klein, A., Bartram, C.R., and Grosveld, G. (1984). Philadelphia chromosomal breakpoints are clustered within a limited region, bcr, on chromosome 22. Cell *36*, 93–99.

Hambardzumyan, D., Becher, O.J., Rosenblum, M.K., Pandolfi, P.P., Manova-Todorova, K., and Holland, E.C. (2008). PI3K pathway regulates survival of cancer stem cells residing in the perivascular niche following radiation in medulloblastoma in vivo. Genes Dev. *22*, 436–448.

Hambardzumyan, D., Amankulor, N.M., Helmy, K.Y., Becher, O.J., and Holland, E.C. (2009). Modeling Adult Gliomas Using RCAS/t-va Technology. Transl. Oncol. *2*, 89–95.

Hoesel, B., and Schmid, J.A. (2013). The complexity of NF-κB signaling in inflammation and cancer. Mol. Cancer *12*, 86.

Holland, E.C., and Varmus, H.E. (1998). Basic fibroblast growth factor induces cell migration and proliferation after glia-specific gene transfer in mice. Proc. Natl. Acad. Sci. USA *95*, 1218–1223.

Holland, E.C., Hively, W.P., DePinho, R.A., and Varmus, H.E. (1998). A constitutively active epidermal growth factor receptor cooperates with disruption of G1 cell-cycle arrest pathways to induce glioma-like lesions in mice. Genes Dev. *12*, 3675–3685.

Holland, E.C., Celestino, J., Dai, C., Schaefer, L., Sawaya, R.E., and Fuller, G.N. (2000). Combined activation of Ras and Akt in neural progenitors induces glioblastoma formation in mice. Nat. Genet. *25*, 55–57.

Huang, B., Yang, X.D., Lamb, A., and Chen, L.F. (2010). Posttranslational modifications of NF-kappaB: another layer of regulation for NF-kappaB signaling pathway. Cell. Signal. *22*, 1282–1290.

Johnson, R.A., Wright, K.D., Poppleton, H., Mohankumar, K.M., Finkelstein, D., Pounds, S.B., Rand, V., Leary, S.E., White, E., Eden, C., et al. (2010). Cross-species genomics matches driver mutations and cell compartments to model ependymoma. Nature *466*, 632–636.

Kim, D., Pertea, G., Trapnell, C., Pimentel, H., Kelley, R., and Salzberg, S.L. (2013). TopHat2: accurate alignment of transcriptomes in the presence of insertions, deletions and gene fusions. Genome Biol. *14*, R36.

Liberski, P.P. (1996). The ultrastructure of ependymoma: personal experience and the review of the literature. Folia Neuropathol. *34*, 212–220.

Louis, D.N., Perry, A., Reifenberger, G., von Deimling, A., Figarella-Branger, D., Cavenee, W.K., Ohgaki, H., Wiestler, O.D., Kleihues, P., and Ellison, D.W. (2016). The 2016 World Health Organization Classification of Tumors of the Central Nervous System: a summary. Acta Neuropathol. *131*, 803–820.

Mack, S.C., Witt, H., Piro, R.M., Gu, L., Zuyderduyn, S., Stütz, A.M., Wang, X., Gallo, M., Garzia, L., Zayne, K., et al. (2014). Epigenomic alterations define lethal CIMP-positive ependymomas of infancy. Nature *506*, 445–450.

Merchant, T.E., Li, C., Xiong, X., Kun, L.E., Boop, F.A., and Sanford, R.A. (2009). Conformal radiotherapy after surgery for paediatric ependymoma: a prospective study. Lancet Oncol. *10*, 258–266.

Mertens, F., Johansson, B., Fioretos, T., and Mitelman, F. (2015). The emerging complexity of gene fusions in cancer. Nat. Rev. Cancer *15*, 371–381.

Mohankumar, K.M., Currle, D.S., White, E., Boulos, N., Dapper, J., Eden, C., Nimmervoll, B., Thiruvenkatam, R., Connelly, M., Kranenburg, T.A., et al. (2015). An in vivo screen identifies ependymoma oncogenes and tumor-suppressor genes. Nat. Genet. *47*, 878–887.

Otero, J.J., Rowitch, D., and Vandenberg, S. (2011). OLIG2 is differentially expressed in pediatric astrocytic and in ependymal neoplasms. J. Neurooncol. *104*, 423–438.

Ozawa, T., Riester, M., Cheng, Y.K., Huse, J.T., Squatrito, M., Helmy, K., Charles, N., Michor, F., and Holland, E.C. (2014). Most human non-GCIMP glioblastoma subtypes evolve from a common proneural-like precursor glioma. Cancer Cell *26*, 288–300.

Pajtler, K.W., Witt, H., Sill, M., Jones, D.T., Hovestadt, V., Kratochwil, F., Wani, K., Tatevossian, R., Punchihewa, C., Johann, P., et al. (2015). Molecular Classification of Ependymal Tumors across All CNS Compartments, Histopathological Grades, and Age Groups. Cancer Cell *27*, 728–743.

Parker, M., Mohankumar, K.M., Punchihewa, C., Weinlich, R., Dalton, J.D., Li, Y., Lee, R., Tatevossian, R.G., Phoenix, T.N., Thiruvenkatam, R., et al. (2014). C11orf95-RELA fusions drive oncogenic NF-κB signalling in ependymoma. Nature *506*, 451–455.

Ritchie, M.E., Phipson, B., Wu, D., Hu, Y., Law, C.W., Shi, W., and Smyth, G.K. (2015). limma powers differential expression analyses for RNA-sequencing and microarray studies. Nucleic Acids Res. *43*, e47.

Rousseau, E., Palm, T., Scaravilli, F., Ruchoux, M.M., Figarella-Branger, D., Salmon, I., Ellison, D., Lacroix, C., Chapon, F., Mikol, J., et al. (2007). Trisomy 19 ependymoma, a newly recognized genetico-histological association, including clear cell ependymoma. Mol. Cancer *6*, 47.

Rudà, R., Gilbert, M., and Soffietti, R. (2008). Ependymomas of the adult: molecular biology and treatment. Curr. Opin. Neurol. *21*, 754–761.

Taylor, M.D., Poppleton, H., Fuller, C., Su, X., Liu, Y., Jensen, P., Magdaleno, S., Dalton, J., Calabrese, C., Board, J., et al. (2005). Radial glia cells are candidate stem cells of ependymoma. Cancer Cell 8, 323–335.

Tzaridis, T., Milde, T., Pajtler, K.W., Bender, S., Jones, D.T., Müller, S., Wittmann, A., Schlotter, M., Kulozik, A.E., Lichter, P., et al. (2016). Low-dose Actinomycin-D treatment re-establishes the tumoursuppressive function of P53 in RELA-positive ependymoma. Oncotarget 7, 61860–61873.

Verstegen, M.J., Leenstra, D.T., Ijlst-Keizers, H., and Bosch, D.A. (2002). Proliferation- and apoptosis-related proteins in intracranial ependymomas: an immunohistochemical analysis. J. Neurooncol. 56, 21–28.

Witt, H., Mack, S.C., Ryzhova, M., Bender, S., Sill, M., Isserlin, R., Benner, A., Hielscher, T., Milde, T., Remke, M., et al. (2011). Delineation of two clinically and molecularly distinct subgroups of posterior fossa ependymoma. Cancer Cell 20, 143–157.